NUMERICAL SIMULATION OF TURBULENCE AND ITS STRUCTURE IN A HYDROCYCLONE①

Chu Liangyin, Chen Wenmei, Li Xiaozhong and Wu Chigong†
Department of Chemical Process Machinery,
† State Key Hydraulics Laboratory of High Speed Flows,
Sichuan Union University, Chengdu 610065, P. R. China

ABSTRACT An Algebraic Stress Turbulence Model (ASM) was introduced into the numerical simulation of the strongly swirling turbulent flow in a hydrocyclone, and the predicted results fit well in the experimental data. The turbulence structure in the hydrocyclone was investigated by combining numerical simulations with experimental studies. The results showed that the radial distributions of the turbulent kinetic energy at different axial positions are similar to each other and can be featured as unsymmetrical saddle-backed curves. The distribution of the turbulent kinetic energy dissipation rate is similar to that of the turbulent kinetic energy. The absolute and relative pressure fluctuations are very large in the inner helical flow and under the vortex finder. The turbulent fluctuating pressures at some positions, especially in the inner helical flow within upper cone section do not fit in Gauss distribution, which indicates that the turbulent fine-structure intermittency exists at these positions.

Key words hydrocyclone numerical simulation of turbulence turbulence structure

1 INTRODUCTION

The structure of turbulence in hydrocyclones has an influence not only on the separation performance but also on the energy consumption, therefore it is necessary to ascertain systematically the turbulence structure for improving the separation performance and reducing the energy consumption. Unfortunately, few investigations have been reported on the structure of turbulence in hydrocyclones. As the computer technology developing with each passing day and the application of turbulence model developing, numerical simulation becomes one of the main methods for studying turbulent flow. Compared with experimental investigation, numerical simulation has some remarkable advantages, such as lower cost and faster and so on. While, some parameters of the turbulence structure, such as turbulence level and probability density distribution characteristics of the turbulent pressure, could not be as yet obtained by numerical simulation but could be measured by experimental study. The systematical investigation of turbulence structure therefore had better be carried out by combining numerical simulation with experimental research. By reviewing the previous achievements, it could be found that there still existed two problems on the numerical simulation of turbulent flow in hydrocyclones. The first one is that the previous numerical simulation investigations paid much attention on the time-averaged velocity field but little on the pressure field and the characteristic parameters of turbulence structure such as turbulent kinetic energy and its dissipation rate. The other one is that in almost all the previous numerical simulation studies the standard $k-\varepsilon$ model was adopted. Even though some simulations made fair predicting precision after modifying the $k-\varepsilon$ model for the anisotropic turbulence in hydrocyclones, the numerical simulation of the strongly swirling turbulent flow in hydrocyclones should adopt the Algebraic Stress Turbulence Model (ASM) instead of the $k-\varepsilon$ model, because the ASM is more benefi-

① Project 96061007 supported by the Doctoral Science Foundation of the State Educational Commission of China and Project No.19 supported by the Postdoctoral Science Foundation of China Received Apr. 13, 1998; accepted Jun. 11, 1998

$$\frac{\partial}{\partial z}(\rho u \varphi) + \frac{1}{r}\frac{\partial}{\partial r}(r\rho u \varphi) = \frac{\partial}{\partial z}(\Gamma_{\varphi z}\frac{\partial \varphi}{\partial z}) - \frac{1}{r}\frac{\partial}{\partial r}(r\Gamma_{\varphi r}\frac{\partial \varphi}{\partial r}) + S_\varphi \quad (9)$$

where φ is the general dependent variable, $\Gamma_{\varphi z}$ and $\Gamma_{\varphi r}$ are transport coefficients of φ in the directions of z and r individually, S_φ is the source term. The expressions of φ, $\Gamma_{\varphi z}$, $\Gamma_{\varphi r}$ and S_φ in every equations are shown in Table 1, where the emerging rate of turbulent kinetic energy G_k is

$$G_k = \overline{u'u'}\frac{\partial u}{\partial z} + \overline{u'v'}(\frac{\partial u}{\partial r} + \frac{\partial v}{\partial z}) + \overline{v'v'}\frac{\partial v}{\partial r} + \overline{u'w'}\frac{\partial w}{\partial z} + \overline{v'w'}[r\frac{\partial}{\partial r}(\frac{w}{r})] + \overline{w'w'}(\frac{v}{r}) \quad (10)$$

where u, v and w are the time-averaged velocities in the direction of z, r and θ respectively.

The values of the constants in the turbulence model mentioned above are taken as follows: $\lambda = 0.2$, $C_k = 0.1$, $C_\varepsilon = 0.1$, $C_{\varepsilon 1} = 1.44$, $C_{\varepsilon 2} = 1.92$, $\sigma_k = 0.5$ and $\sigma_\varepsilon = 1.33$.

Table 1 Formulations of φ, $\Gamma_{\varphi z}$, $\Gamma_{\varphi r}$ and S_φ in equation (9)

Equation	φ	$\Gamma_{\varphi z}$	$\Gamma_{\varphi r}$	S_φ
Continuity	1	0	0	0
z-momentum	u	$2\lambda\rho\frac{k}{\varepsilon}\overline{u'u'} + 2\mu$	$\lambda\rho\frac{k}{\varepsilon}\overline{v'v'} + \mu$	$-\frac{\partial p}{\partial z} - \frac{\partial}{\partial z}[\frac{2}{3}(1-\lambda)\rho k - 2\lambda\rho\frac{k}{\varepsilon}\overline{u'v'}\frac{\partial u}{\partial r} + \frac{1}{r}\frac{\partial u}{\partial r}(-r\lambda\rho\frac{k}{\varepsilon}\overline{u'w'}\frac{w}{r})]$
r-momentum	v	$\lambda\rho\frac{k}{\varepsilon}\overline{u'u'} + \mu$	$2\lambda\rho\frac{k}{\varepsilon}\overline{v'v'} + 2\mu$	$-\frac{\partial p}{\partial r} + \frac{\partial}{\partial z}(\mu\frac{\partial \mu}{\partial r}) - 2\mu\frac{v}{r^2} + \rho\frac{w^2}{r} + \rho\frac{\overline{w'w'}}{r} + \frac{\partial}{\partial z}[\lambda\rho\frac{k}{\varepsilon}(\overline{v'v'}\frac{\partial u}{\partial r} - \overline{u'w'}\frac{w}{r})] + \frac{1}{r}\frac{\partial}{\partial r}[-\frac{2}{3}r\rho k(1-\lambda)]$
θ-momentum	w	$\lambda\rho\frac{k}{\varepsilon}\overline{u'u'} + \mu$	$\lambda\rho\frac{k}{\varepsilon}\overline{u'u'} + 2\mu$	$-\rho\frac{vw}{r} - \rho\frac{\overline{v'w'}}{r} - \frac{w}{r^2}\frac{\partial}{\partial r}(r\mu) + \frac{\partial}{\partial z}(\lambda\rho\frac{k}{\varepsilon}\overline{u'v'}\frac{\partial w}{\partial r})$
Turbulent kinetic energy	k	$C_k\rho\frac{k^2}{\varepsilon} + \frac{\mu}{\sigma_k}$	$C_k\rho\frac{k^2}{\varepsilon} + \frac{\mu}{\sigma_k}$	$G_k - \rho\varepsilon$
Turbulent kinetic energy dissipation rate	ε	$C_\varepsilon\rho\frac{k^2}{\varepsilon} + \frac{\mu}{\sigma_k}$	$C_\varepsilon\rho\frac{k^2}{\varepsilon} + \frac{\mu}{\sigma_\varepsilon}$	$\frac{\varepsilon}{k}(C_{\varepsilon 1}C_k - C_{\varepsilon 2}\rho\varepsilon)$

3 NUMERICAL METHOD OF SOLUTION

3.1 Boundary conditions

3.1.1 Inlet boundary

The radial coordinate of the hydrocyclone inlet varies with θ, if it was described with a three-dimensional coordinate system, the calculation will be very complex. Fortunately, the flow inside the hydrocyclone could be considered as two-dimensional turbulent elliptic flow because the flow is axisymmetric. Therefore, the three-dimensional geometric boundary of the inlet could be simplified as two-dimensional circumferential inlet, i.e., the inlet fluid flows into the hydrocyclone evenly from the circumference. Then, the inlet condition could be stated as

$$u_e = 0,\ w_e = \frac{4Q_e}{\pi d_e^2},\ v_e = \frac{Q_e}{\pi d_e D},\ k_e = 0.01\,w_e^2,\ \varepsilon_e = \frac{k_e^{1.5}}{0.04} \quad (11)$$

where Q_e is the hydrocyclone capacity, d_e and D are inlet diameter and hydrocyclone diameter individually.

3.1.2 Outlet boundary

At the entrance of vortex finder and apex, the fluid flow could be taken as fully developed turbulent flow. Then, the outlet condition may be assumed as that the gradients of all properties are zero, i.e.

are proper for the computation of flow field in the hydrocyclone to get satisfactory predicting results.

4.2 Structure of turbulence

4.2.1 Turbulent kinetic energy

The predicted turbulent kinetic energy profiles in the hydrocyclone is shown in Fig.2. The results show that the radial distributions of the turbulent kinetic energy at different axial positions under the vortex finder are similar and featured as unsymmetrical saddle-backed curves where the turbulent kinetic energy near the air core is large, while the radial distribution of the turbulent kinetic energy in the ring space between the vortex finder wall and the hydrocyclone wall varies little. The turbulent kinetic energy is very large in the inner helical flow near the air core and under the vortex finder.

The turbulent kinetic energy mainly comes from time-averaged flow and provides energy for turbulence[9]. The distribution of turbulent kinetic energy in the hydrocyclone indicates that much energy is transited from the time-averaged flow to the turbulent flow in the space that in the inner helical flow near the air core and under the vortex finder and in the space near the hydrocyclone wall, i.e., much energy of the time-averaged flow is lost in these two regions because of the turbulent flow and the energy loss is much large in the region that in the inner helical flow near the air core.

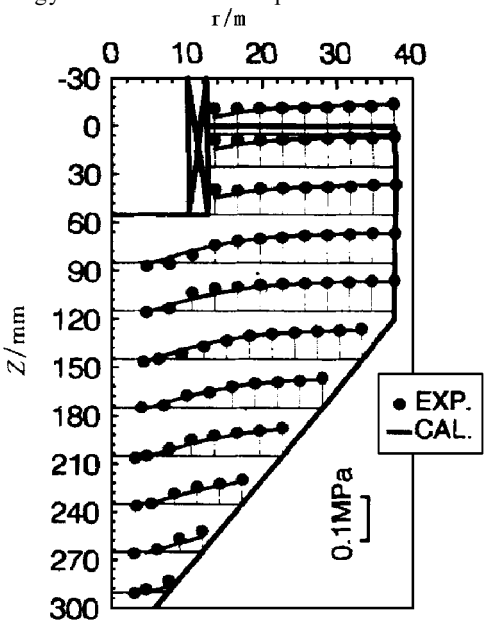

Fig.1 Comparison of predicted pressure profiles with experimental results
r—Radius; Z—Axial position

4.2.2 Turbulent kinetic energy dissipation rate

The predicted turbulent kinetic energy dissipation rate profiles in the hydrocyclone is shown in Fig.3. Comparing the result in Fig.3 with that in Fig.2, we find that the distribution of the turbulent kinetic energy dissipation rate is similar to that of the turbulent kinetic energy, i.e., the turbulent kinetic energy dissipation rate is also large in the inner helical flow near the air core and under the vortex finder.

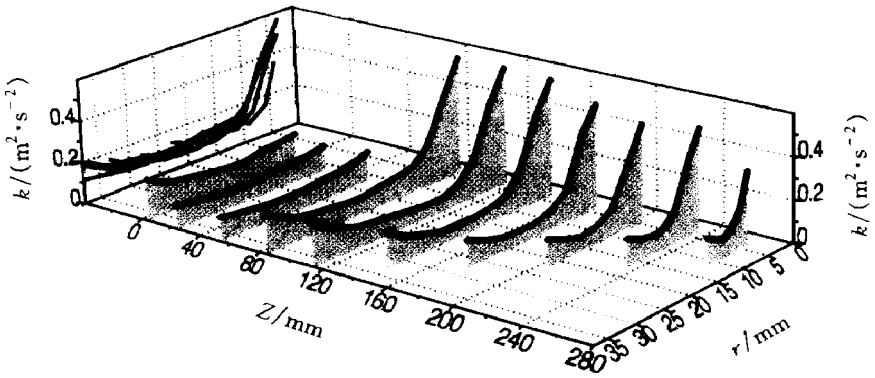

Fig.2 Predicted turbulent kinetic energy (*k*) profiles
r—Radius; Z—Axial position

4.2.3 Pressure fluctuation and relative pressure fluctuation

1 % in the space mentioned above. Whereas, in the space where the radius of a position is smaller than that of the outside wall of vortex finder, the relative pressure fluctuation increases sharply with the radius of position reducing no matter how the axial position varies. In the middle and upper space of cone section, the relative pressure fluctuation increases sharply especially. This indicates that the ratio of the energy taken by turbulent flow from time-averaged flow to the total energy in time-averaged flow is very large in the inner helical flow and under the vortex finder. At some positions, the above ratio is as high as 60 %.

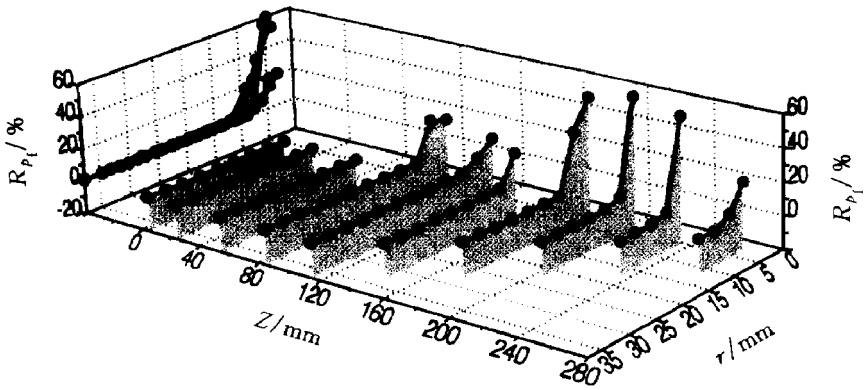

Fig.5 Three dimenisional carpet plot of relative pressure fluctuation (R_{p_f})

r —Radius; Z —Axial position

4.2.4 Probability density distribution characteristics of turbulent pressure and internal intermittency of turbulence

The probability distributions of the turbulent fluctuating properties in a really stochastic and isotropic turbulent flow field should fit in Gauss distribution[9], but actually a general turbulent flow field is not a Gaussian stochastic field[2]. The phenomenon that the probability distributions of the turbulent fluctuating properties do not fit in Gauss distribution is the display of internal intermittency of turbulence. The internal intermittency of turbulence, which is also called fine-structure intermittency, means that some physical properties especially some high-order statistical properties in the fully developed turbulent flow field do not exist at every point of space or time, i.e., the properties have curiosity[11]. To quantitatively describe the deviation of a statistical totality from Gauss distribution, two characteristic coefficients called skewness coefficient and kurtosis coefficient are defined as follows[12]:

$$B_s = \frac{\mu_3}{\sigma^3}, \quad B_k = \frac{\mu_4}{\sigma^4} \tag{14}$$

where B_s is the skewness coefficient which is used to describe the skewness of the distribution, μ_3 is the three-order central matrix of the totality, σ is the standard deviation of the totality, B_k is the kurtosis coefficient which is used to describe the kurtosis of the distribution, and μ_4 is the four-order central matrix of the totality.

For the Gauss distribution, the skewness coefficient and kurtosis coefficient are $B_s = 0$ and $B_k = 3$. Therefore, the skewness coefficient and kurtosis coefficient could be used jointly to describe the total deviation of the statistical totality from Gauss distribution and test whether the totality fits in Gauss distribution or not.

The skewness coefficient and kurtosis coefficient and Gauss distribution test of turbulent fluctuating pressure in the hydrocyclone are shown in Table 2, where the symbol "Yes" stands for that the turbulent fluctuating pressure fits in Gauss distribution. The Gauss distribution test is carried out ac-

turbulence mathematical model and numerical method of solution were verified experimentally, the predicted results fit well in the experimental data.

(2) The radial distributions of the turbulent kinetic energy at different axial positions under the vortex finder are similar and featured as unsymmetrical saddle-backed curves, the turbulent kinetic energy near the air core is large, while the radial distribution of the turbulent kinetic energy in the ring space between vortex finder wall and hydrocyclone wall varies little. The distribution of the turbulent kinetic energy dissipation rate is similar to that of the turbulent kinetic energy, i.e., the turbulent kinetic energy dissipation rate is also large in the inner helical flow near the air core and under the vortex finder.

(3) Both the pressure fluctuation and the relative pressure fluctuation of the turbulent flow are very large in the inner helical flow and under the vortex finder, i.e., the turbulent energy dissipation is very large in that area.

(4) The turbulent fluctuating pressures in the main space inside hydrocyclones fit in Gauss distribution, but the turbulent fluctuating pressures at some positions in the cylindrical section and in the inner helical flow within upper cone section do not fit in Gauss distribution, which indicates that the turbulent fine-structure intermittency exists at these positions.

REFERENCES

1 Zhou Lixing. Numerical Simulation of Turbulent Two-Phase Flow and Combustion. Beijing: Qinghua University Press, 1991. 8.
2 Shi Xungang. Turbulence. Tianjin: Tianjin University Press, 1994: 3.
3 Rodi W. ZAMM, 1976, 56: 7219 - 7221.
4 Launder B E and Spalding B E. Comp Meths Appl Mech Eng, 1974, 3:269.
5 Patanker S V and Spalding D B. Int J Heat and Mass Transfer, 1972, 15: 1787 - 1806.
6 Patanker S V. Numerical Heat Transfer and Fluid Flow. New York: McGraw-Hill, 1980.
7 Ames W F. Numerical Methods for Partial Differential Equations. 2nd ed. New York: Academic Press, 1977: 145 - 151.
8 Rietema K. Chem Engng Science, 1961, 15(3/4):320 - 325.
9 Du Guoren. Turbulent Fluid Mechanics (Part I). Beijing: People's Education Press, 1981: 11.
10 Hinze J O. Turbulence. 2nd ed. New York: McGraw-Hill Book Company, 1979.
11 Hu Fei. Turbulence, Intermittency and Boundary Layer of Atmosphere. Beijing: Science Press, 1995: 9.
12 Ma Fengshi, He Liangcai, Yu Mingshu *et al*. Applied Probability Statistics. Beijing: Higher Education Press, 1989.

(Edited by Wu Jiaquan)

cial to better predicting precision[1]. As a result, an Algebraic Stress Turbulence Model is introduced into the numerical simulation of turbulent flow, and a resistance wire strain gauge system is used to experimentally study the turbulent pressure field in the hydrocyclone, then the structure of turbulence is ascertained systematically.

2 TURBULENCE MODEL

2.1 Basic equations

Continuity equation

$$\frac{\partial U_i}{\partial x_i} = 0 \tag{1}$$

Navier-Stokes equation

$$\frac{\partial U_i}{\partial t} + U_j \frac{\partial U_i}{\partial x_j} = -\frac{1}{\rho}\frac{\partial p}{\partial x_i} + \frac{\partial}{\partial x_j}[\nu \frac{\partial U_i}{\partial x_j} - \overline{u'_i u'_j}] + g_i \tag{2}$$

Reynolds stress equation

$$\frac{\partial}{\partial t}(\overline{u'_i u'_j}) + U_l \frac{\partial \overline{u'_i u'_j}}{\partial x_l} = \frac{\partial}{\partial x_l}[-\overline{u'_i u'_j u'_l} - \overline{\frac{p'}{\rho}(\delta_{jl} u'_i + \delta_{il} u'_j)} + \nu \frac{\partial \overline{u'_i u'_j}}{\partial x_l}] - (\overline{u'_i u'_l}\frac{\partial U_j}{\partial x_l} + \overline{u'_j u'_l}\frac{\partial U_i}{\partial x_l}) - 2\nu \overline{\frac{\partial u'_i}{\partial x_l}\frac{\partial u'_j}{\partial x_l}} + \overline{\frac{p'}{\rho}(\frac{\partial u'_i}{\partial x_j} + \frac{\partial u'_j}{\partial x_i})} \tag{3}$$

Turbulent kinetic energy equation

$$\frac{\partial k}{\partial t} + U_l \frac{\partial k}{\partial x_l} = \frac{\partial}{\partial x_l}[-\overline{u'_l(k' + \frac{p'}{\rho})} + \nu \frac{\partial k}{\partial x_l}] - \overline{u'_i u'_l}\frac{\partial U_i}{\partial x_l} - \varepsilon \tag{4}$$

Turbulent kinetic energy dissipation rate equation

$$\frac{\partial \varepsilon}{\partial t} + U_l \frac{\partial \varepsilon}{\partial x_l} = \frac{\partial}{\partial x_l}[-\overline{\varepsilon' u'_l} - \frac{2\nu}{\rho}\overline{\frac{\partial p'}{\partial x_j}\frac{\partial u'_l}{\partial x_j}} + \nu \frac{\partial \varepsilon}{\partial x_l}] - 2\nu \frac{\partial U_i}{\partial x_j}(\overline{\frac{\partial u'_l}{\partial x_i}\frac{\partial u'_l}{\partial x_j}} + \overline{\frac{\partial u'_i}{\partial x_l}\frac{\partial u'_j}{\partial x_l}}) - 2\nu \overline{u'_l \frac{\partial u'_i}{\partial x_j}\frac{\partial^2 U_i}{\partial x_i \partial x_j}} - 2\nu \overline{\frac{\partial u'_i}{\partial x_j}\frac{\partial u'_i}{\partial x_l}\frac{\partial u'_j}{\partial x_l}} - 2(\nu \overline{\frac{\partial^2 u_i}{\partial x_l \partial x_j}})^2 \tag{5}$$

2.2 Set of equations of Algebraic Stress Turbulence Model (ASM)

The above basic turbulent equations are not closed yet, some equations have to be modeled. After modeling, the turbulent kinetic energy equation and turbulent kinetic energy dissipation rate equation have the following forms[1,2]

$$\frac{\partial k}{\partial t} + U_l \frac{\partial k}{\partial x_l} = \frac{\partial}{\partial x_l}(C_k \frac{k}{\varepsilon}\overline{u'_i u'_l}\frac{\partial k}{\partial x_i} + \nu \frac{\partial k}{\partial x_l}) - \overline{u'_i u'_l}\frac{\partial U_i}{\partial x_l} - \varepsilon \tag{6}$$

$$\frac{\partial \varepsilon}{\partial t} + U_l \frac{\partial \varepsilon}{\partial x_l} = \frac{\partial}{\partial x_l}(C_\varepsilon \frac{k}{\varepsilon}\overline{u'_i u'_l}\frac{\partial \varepsilon}{\partial x_i} + \nu \frac{\partial \varepsilon}{\partial x_l}) - (\overline{u'_i u'_l}\frac{\partial U_i}{\partial x_l}C_{\varepsilon 1} + C_{\varepsilon 2}\varepsilon)\frac{\varepsilon}{k} \tag{7}$$

Reynolds stress equation could be simplified as algebraic equation by treating the transport terms with the Rodi approximation[3]:

$$\overline{u'_i u'_j} = (1 - \lambda)\frac{2}{3}\delta_{ij}k - \lambda \frac{k}{\varepsilon}(\overline{u'_i u'_l}\frac{\partial U_j}{\partial x_l} + \overline{u'_j u'_l}\frac{\partial U_i}{\partial x_l}) \tag{8}$$

where λ is a constant, and δ_{ij} is the Kronecker function, $\delta_{ij} = 1$ when $i = j$, and $\delta_{ij} = 0$ when $i \neq j$.

Then, the closed set of equations of ASM are composed of Equations (1), (2), (6), (7) and (8).

The time-averaged flow equations and $k-\varepsilon$ equations in the cylindrical coordinate system could be described as follows by changing the time-averaged flow equations into the form of Boussinesq Equation and taking the diffusion term in $k-\varepsilon$ equations as an isotropic term[1]:

$$\frac{\partial u}{\partial z} = 0, \frac{\partial v}{\partial z} = 0, \frac{\partial w}{\partial z} = 0, \frac{\partial k}{\partial z} = 0, \frac{\partial \varepsilon}{\partial z} = 0 \tag{12}$$

3.1.3 Air-core boundary

The air core boundary condition could be expressed as follows by approximating the air-water interface as a stable, symmetric and unmovable cylindrical surface.

$$v \cdot n = 0, \frac{\partial u}{\partial r} = 0, \quad v = 0, \frac{\partial w}{\partial r} = 0, \frac{\partial k}{\partial r} = 0, \frac{\partial \varepsilon}{\partial r} = 0 \tag{13}$$

where n is the unit vector in the normal direction.

3.1.4 Solid wall boundary

At walls, all fluxes, but diffusion of momentum due to velocity parallel to the wall, are zero. In the near-wall region, the Wall-Function method[4] is used to "bridge" the gap between the fully turbulent region and the wall. The distributions of velocity and turbulent kinetic energy and turbulent kinetic energy dissipation rate in the viscous near-wall layer are all gotten by using the Wall-Function method.

3.2 Numerical method of solution

The numerical method of solution is based on the SIMPLE (Semi-Implicit Method for Pressure-Linked Equations)[5] algorithm and with three features as following: (1) the flow field is divided into many control volumes; (2) the model equations are integrated in each control volume; and (3) the differential transport equation is converted into a set of algebraic finite-difference equations by discretization and then the discrete properties of the flow field are worked out. A staggered grid system and the control volume method are used for the discretization of the set of differential equations. The SIMPLER (SIMPLE Revised)[6] algorithm is considered here for handling the velocity-pressure linkage and the set of algebraic equations are solved by a line-iterative method using an ADI (Alternating Direction Implicit)[7] algorithm with alternating sweep directions.

4 COMPUTATIONAL AND EXPERIMENTAL RESULTS

4.1 Computation parameters design and experimental verification

The geometric parameters of hydrocyclone with d 75 mm were designed according to Rietema[8] optimum hydrocyclone geometry for separation. To reduce the CPU time and ensure the calculation precision at the same time, the grid divisions were designed denser in the region where the gradients of properties are larger such as in the inner helical flow region and the region nearby the entrance with the distance between radial grid divisions being 1.5 mm and that between axial grid divisions being 5 mm nearby the entrance; and the grid divisions were smaller in other region with the distance between radial grid divisions being 3 mm and that between axial grid divisions being 15 mm.

To verify the computational results and to get some characteristic parameters of turbulence structure that could not be gotten by numerical simulation, experimental investigation was carried out on the turbulent pressure field. The measuring instrument was a resistance wire strain gauge system which is mainly composed of pressure probe, resistance wire strain type pressure sensor, amplifier, A/D converter, digital display, computer, printer and related measuring software. The experimental fluid was water. The distribution of measured points in the hydrocyclone was featured with grid nodes described as follows: the axial distances from the hydrocyclone top were 5, 25, 55, 85, 115, 145, 175, 205, 235, 265 and 290 mm, and the radial step was 3 mm. The hydrocyclone inlet pressure was 0.08 MPa constantly in the experiments. The capacity of the hydrocyclone was measured by an electromagnetic flowmeter.

The comparison of predicted pressure profiles with experimental results in the hydrocyclone is shown in Fig.1. It could be found that the predicted results fit well in the experimental data, which indicates that the above described turbulence mathematical model and the numerical method of solution

Pressure fluctuation is defined as the standard deviation of the turbulent fluctuating pressure. Relative pressure fluctuation is defined as the ratio of the standard deviation of the turbulent fluctuating pressure to the time-averaged pressure. According to the energy transition, turbulent flow takes energy from time-averaged flow to maintain the turbulence[10]. The dimensions of the pressure fluctuation depend on the absolute value of the energy taken by turbulent flow from time-averaged flow, and the dimensions of the relative pressure fluctuation is related to the ratio of the energy taken by turbulent flow from time-averaged flow to the total energy in time-averaged flow.

The three dimenisional carpet plot of pressure fluctuation in the hydrocyclone is shown in Fig.4. The results indicate that the pressure fluctuation decreases near the wall, maintains a relative stable level and increases sharply near the air core. That is, the distributions of pressure fluctuation at different axial positions are similar and featured as unsymmetrical saddle-backed curves where the pressure fluctuation near the air core is large. The pressure fluctuation is very large in the inner helical flow and under the vortex finder.

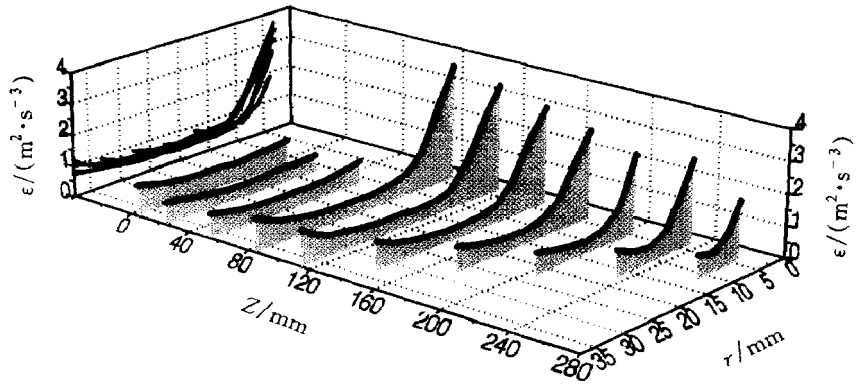

Fig.3 Predicted turbulent kinetic energy dissipation rate (ε) profiles
r—Radius; Z—Axial position

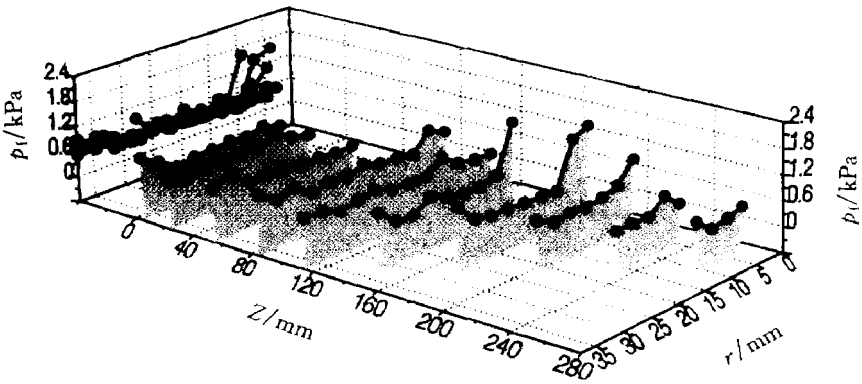

Fig.4 Three dimenisional carpet plot of pressure fluctuation (p_f)
r—Radius; Z—Axial position

Fig.5 is the three dimenisional carpet plot of relative pressure fluctuation in the hydrocyclone. In the space outside the wall of vortex finder, the relative pressure fluctuation level is stably within the limits of 0.6 % ~ 1 % no matter how the axial position varies, i.e., the ratio of the energy taken by turbulent flow from time-averaged flow to the total energy in time-averaged flow is as small as 0.6 % ~

cording to the combination of skewness coefficient with kurtosis coefficient. Taking ($|B_s|$, B_k) as the coordinate point, if the point is nearby the point (0, 3), the distribution could be considered as Gauss distribution; otherwise, the distribution could not be taken as Gauss distribution. The results of Gauss distribution tests of turbulent fluctuating pressures in Table 2 are gotten under the featured level at $\alpha = 0.01$. The turbulent fluctuating pressures in the main space inside hydrocyclones fit in Gauss distribution, but the turbulent fluctuating pressures at some positions in the cylindrical section and in the inner helical flow within upper cone section do not fit in Gauss distribution, which indicates that the turbulent fine-structure intermittency exists at these positions in the hydrocyclone.

Table 2 Skewness coefficient (B_s) and kurtosis coefficient (B_k) and Gauss distribution (G.D.) test of turbulent fluctuating pressure in hydrocyclone

Axial position Z/ mm	Item	Radial position, r/ mm											
		4.5	7.5	10.5	13.5	16.5	19.5	22.5	25.5	28.5	31.5	34.5	37.5
5	B_s				0.267	-0.344	0.077	0.144	-0.041	-0.165	0.113	0.350	0.951
	B_k				2.509	2.526	2.500	2.810	2.798	2.942	2.679	2.298	4.334
	G.D.				Yes	Yes	Yes	Yes	Yes	Yes	Yes	Yes	No
25	B_s				0.409	0.380	1.036	-0.199	0.268	0.013	0.148	0.199	0.100
	B_k				2.670	2.496	3.643	2.498	3.078	2.516	2.408	2.757	2.909
	G.D.				Yes	Yes	No	Yes	Yes	Yes	Yes	Yes	Yes
55	B_s				0.090	-0.066	0.329	-0.799	0.053	-0.038	-0.356	-0.300	-0.006
	B_k				2.467	2.575	2.877	4.789	2.543	2.413	2.679	2.496	2.258
	G.D.				Yes	Yes	Yes	No	Yes	Yes	Yes	Yes	Yes
85	B_s	-0.769	-0.238	0.019	-0.074	-0.112	-0.500	-0.113	0.143	0.032	0.048	-0.183	1.401
	B_k	4.001	2.426	2.217	2.735	2.731	2.813	2.515	2.205	2.254	3.432	2.473	5.698
	G.D.	No	Yes	Yes	Yes	Yes	Yes	Yes	Yes	Yes	Yes	Yes	No
115	B_s	0.198	-0.149	0.392	-0.329	-0.181	0.225	0.117	0.179	0.033	0.133	-0.129	0.091
	B_k	2.758	2.582	2.796	2.151	2.712	2.774	2.600	2.139	2.643	2.540	2.284	2.368
	G.D.	Yes	Yes	Yes	Yes	Yes	Yes	Yes	Yes	Yes	Yes	Yes	Yes
145	B_s	0.211	0.061	1.007	-0.777	-0.223	-0.064	-0.185	0.128	-0.101	0.152	0.524	
	B_k	2.661	2.467	2.673	2.865	2.483	3.118	2.384	2.315	2.609	2.532	2.392	
	G.D.	Yes	Yes	No	No	Yes	Yes	Yes	Yes	Yes	Yes	Yes	
175	B_s	0.089	0.152	-0.648	0.194	0.089	0.129	-0.003	-0.256	1.266			
	B_k	2.731	1.847	2.271	2.278	2.231	2.849	2.430	2.428	4.966			
	G.D.	Yes	No	No	Yes	Yes	Yes	Yes	Yes	No			
205	B_s	0.064	-0.327	-0.822	0.051	-0.229	0.254	0.111	0.347				
	B_k	2.857	1.902	2.800	3.136	2.381	2.412	2.332	2.233				
	G.D.	Yes	No	No	Yes	Yes	Yes	Yes	Yes				
235	B_s	0.045	-0.475	-0.052	0.075	0.215	0.019						
	B_k	1.899	2.755	2.622	2.546	2.576	2.464						
	G.D.	No	Yes	Yes	Yes	Yes	Yes						
265	B_s	-0.419	0.241	-0.473	-0.018	-0.151							
	B_k	2.711	2.458	3.122	2.460	2.381							
	G.D.	Yes	Yes	Yes	Yes	Yes							

5 CONCLUSIONS

(1) Numerical simulation of the turbulent flow in a hydrocyclone was carried out successfully with an Algebraic Stress Turbulence Model (ASM) in the cylindrical coordinate system, and the established